Lasing in Thue–Morse structures with optimized aperiodicity

Heeso Noh,[1] Jin-Kyu Yang,[1] Svetlana V. Boriskina,[2] Michael J. Rooks,[1] Glenn S. Solomon,[3] Luca Dal Negro,[2,4,a)] and Hui Cao[1,a)]
[1]*Department of Applied Physics, Yale University, New Haven, Connecticut 06511, USA*
[2]*Department of Electrical and Computer Engineering and Photonics Center, Boston University, Boston, Massachusetts 02215, USA*
[3]*Joint Quantum Institute, NIST, University of Maryland, Gaithersburg, Maryland 20899, USA*
[4]*Division of Materials Science and Engineering, Boston University, Brookline, Massachusetts 02446, USA*

(Received 13 March 2011; accepted 27 April 2011; published online 19 May 2011)

We demonstrate lasing in two-dimensional Thue–Morse structures fabricated in a semiconductor membrane. By changing the relative size of two scatterers that correspond to the building blocks *A* and *B*, we gradually vary structural aperiodicity and find an optimal degree of aperiodicity where light confinement is maximal and lasing is the strongest. At various degrees of aperiodicity, different types of modes acquire the highest quality factors and may be selected for lasing. This work opens a way of controlling lasing characteristic via structural aperiodicity. © *2011 American Institute of Physics*. [doi:10.1063/1.3592850]

Aperiodic photonic structures can be generated by deterministic rules and posses long-range order.[1,2] Unlike periodic or quasiperiodic structure, deterministic aperiodic structures lack both translational and rotational symmetries. A principal example is given by the Thue–Morse (Th–Mo) structure, which is generated by two symbols, *A* and *B*, following the inflation rule: $A \rightarrow AB$ and $B \rightarrow BA$.[3,4] The successive Th–Mo strings are *A*, *AB*, *ABBA*, *ABBABAAB*, etc. The spatial Fourier power spectrum of an infinitely long Th–Mo structure is singular continuous,[1] in contrast to the singular (δ function) Fourier spectra of periodic and quasiperiodic lattices. Consequently, photonic band gaps (PBGs) and light transport in Th–Mo structures display unusual properties, e.g., fractal gaps, anomalous diffusion.[5–7] Resonant transmission and frequency trifurcation have been reported in Th–Mo multistack layers.[4,8] Omnidirectional reflection and photoluminescence enhancement are also demonstrated.[9–11] Recently the Th–Mo inflation method has been generalized from one-dimensional sequence to two dimensional (2D),[12,13] $A \rightarrow \binom{A\ B}{B\ A}$ and $B \rightarrow \binom{B\ A}{A\ B}$. *A* (or *B*) stands for the presence (or absence) of a dielectric/metallic scatterer on a 2D square lattice. Such structure is shown to support critical states that lie in between localized states and extended states.[14,15] However, lasing in Th–Mo structures have not been explored so far.

In this letter, we investigate experimentally and numerically lasing behavior in 2D Th–Mo structures. Instead of removing scatterers from a square lattice following the Th–Mo inflation rule, we modulate the size of scatterers on the square lattice, namely, *A* and *B* represent scatterers of different size. Varying their size ratio *b* induces a gradual transition from aperiodic ($b=0$) to periodic ($b=1$) systems. Maximal light confinement in quasi-2D Th–Mo membranes is achieved at an intermediate value $0<b<1$, where lasing becomes the strongest.

The 2D Th–Mo structures are fabricated on a GaAs membrane that is free standing in air. The membrane is 190 nm thick and contains three uncoupled layers of InAs quantum dots (QDs). Circular holes are etched into the layer via e-beam lithography and reactive ion etching. The sample fabrication procedure is similar to that described in Ref. 16. The two different size air holes are arranged according to the 2D Th–Mo sequence, corresponding to the building blocks *A* and *B* on a square lattice. The lattice constant is $a=320$ nm. The lateral dimension of the pattern is 20 μm $\times$ 20 μm or equivalently $64a \times 64a$. The radius R_1 for *A* is fixed while R_2 for *B* is varied. Figure 1 shows two fabricated structures with $b=R_2/R_1=0.83$ and 0.67. Their spatial Fourier spectra exhibit primary peaks that correspond to the reciprocal vectors of the square lattice. In addition, there is a large density of spatial frequency components that result from structural aperiodicity. They form a nearly continuous background when the structure size is large enough. As *b* increases toward 1, the structural aperiodicity is reduced, and the continuous background of the spatial Fourier spectra diminishes.

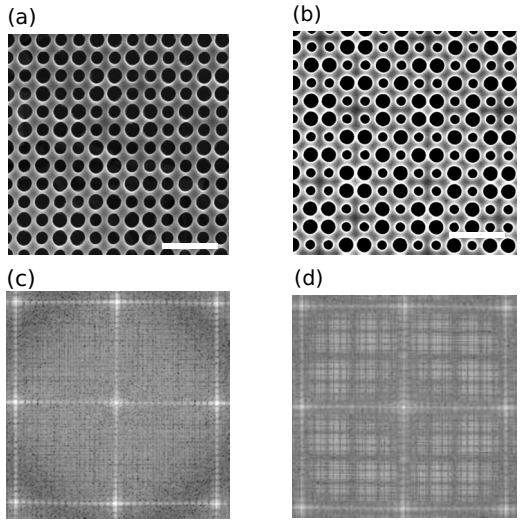

FIG. 1. [(a) and (b)] Top-view scanning electron microscope (SEM) images of parts of Th–Mo patterns fabricated in a GaAs membrane. Air holes of radii R_1 and R_2 are arranged in 2D Th–Mo sequence. $R_1=130$ nm and $R_2=108$ nm in (a) and 87 nm in (b). The scale bar is 1 μm. [(c) and (d)] Reciprocal space representations of the structures (a) and (b) obtained by Fourier transform of the SEM images. Besides the primary peaks that correspond to the square lattice, there are many secondary peaks due to structural aperiodicity, which become weaker as R_2 approaches R_1.

a)Authors to whom correspondence should be addressed. Electronic addresses: hui.cao@yale.edu and dalnegro@bu.edu.

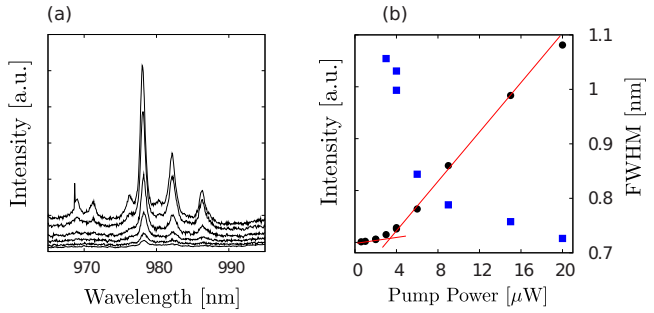

FIG. 2. (Color online) (a) Emission spectra taken at the incident pump power $P=3,\ 4.1,\ 6,\ 9,\ 15,\ 20\ \mu$W. (b) Measured intensity (black circle) and spectral width (blue square) of one emission peak at wavelength $\lambda=978$ nm vs P showing the onset of lasing at $\sim 3\ \mu$W. The solid lines are linear fitting of peak intensity below and above the threshold pump power ($\sim 3\ \mu$W).

The lasing experimental setup is the same as that in Ref. 16. Femtosecond pulses from a mode-locked Ti:Sapphire laser are used to excite the InAs QDs. The pump spot has a diameter $\sim 3\ \mu$m. Figure 2(a) shows a series of emission spectra taken at different pump levels. The emission peaks grow with the incident pump power P. Figure 2(b) plots the intensity of one peak at wavelength $\lambda=978$ nm as a function of P. The data (solid black circle) display a clear threshold behavior. Above the pump power $\sim 3\ \mu$W, the peak intensity grows much more rapidly with P. Meanwhile the peak width (full width at half maximum) decreases monotonically with increasing P. It experiences a quick drop around the threshold pump power $\sim 3\ \mu$W, and eventually reaches the value of 0.71 nm at high pumping $P=20\ \mu$W. These data demonstrate the onset of lasing at $P \simeq 3\ \mu$W. We have observed numerous lasing modes as we scan the pump spot across the 2D Th–Mo structure. The lasing threshold varies from mode to mode. The frequencies of lasing peaks vary with the pump positions, indicating the lasing modes are spatially localized in the 2D Th–Mo structure.

Next we probe lasing in several Th–Mo patterns of different ratio $b=R_2/R_1$. The lattice constant a is set at 300 nm and R_1 at 114 nm, while R_2 changes from 93 nm to 69 nm, and 45 nm. Among them, the structures of $R_2=69$ nm ($b=0.61$) demonstrate the strongest lasing, namely, the lasing peaks are the highest under identical pump condition. We also fabricate samples of $b=0$, but could not achieve lasing with the maximum power of our pump source.

To understand the lasing behavior in the Th–Mo structures, we perform three-dimensional numerical simulation with a commercial program (COMSOL MULTIPHYSICS 3.5). The thickness of the GaAs membrane is identical to the experimental value, and the refractive index of GaAs is 3.4. Since the lasing modes usually correspond to high-quality (Q) resonances of the passive system, we compute such resonances within the frequency range of laser emission. Our simulation is limited to the transverse-electric (TE) polarization (electric field parallel to the membrane) because the lasing modes are TE-polarized due to stronger index guiding and preferential gain of InAs QDs for TE modes. We fix R_1 at $0.4a$ and change R_2 from 0 to $0.4a$ with a step of $0.05a$. Due to limited computer memory, the lateral dimension of the structure is $16a \times 16a$, significantly smaller than that of the real samples. Hence, our numerical simulation aims to provide qualitative instead of quantitative explanation for the experimental results. For each value of b, we find the highest-Q factor for all modes with the frequency range of interest. Its value is plotted against b in Fig. 3(a). The global maximum of Q is reached at $b=0.75$. Hence, there is an optimal value of b where the overall Q factor is maximized. This result explains the experimental observation of strongest lasing at an intermediate value of b between 0 and 1. However, the exact value of optimal b depends on the pattern size. Moreover, the maximal Q increases with the pattern size, thus we expect a much higher Q for the lasing modes in the real structures.

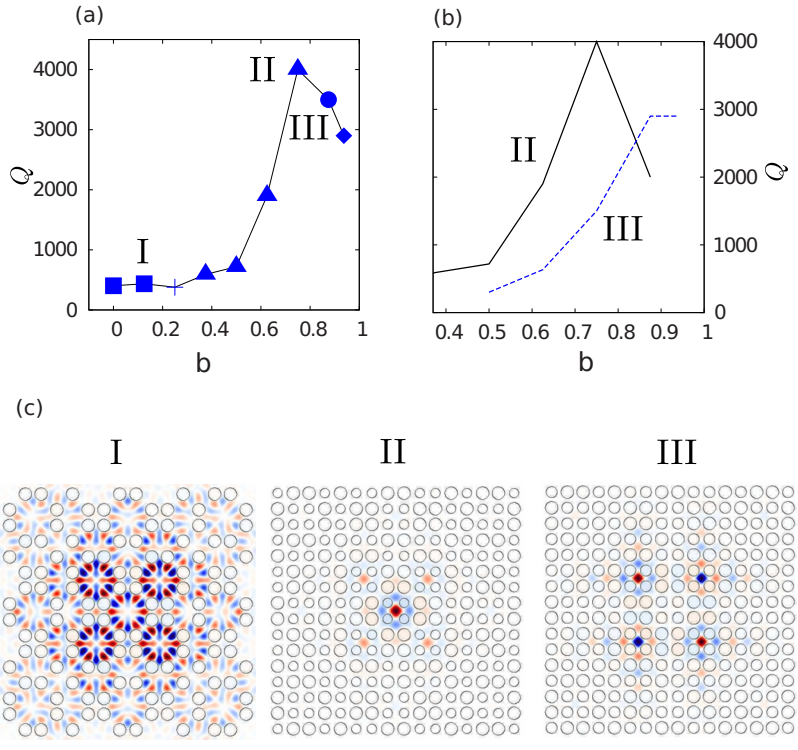

FIG. 3. (Color online) (a) Calculated Q values of the highest-Q modes for each b. Different symbols represent different types of modes, e.g., square for type I, triangle for type II, and circle for type III. (b) Q factor as a function of b for type II (black curve) and III (blue dashed curve) modes. (c) Spatial distribution of magnetic field for type I, II, and III modes (from left to right). Type II becomes the overall maximal-Q mode at $b=0.75$.

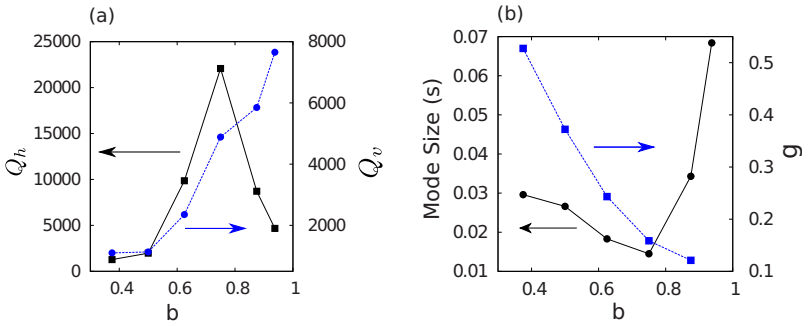

FIG. 4. (Color online) (a) Calculated Q_h and Q_v for the highest-Q modes vs b. Q_h becomes maximal at $b=0.75$ while Q_v increases monotonically with b. (b) Lateral size s of the highest-Q mode and percentage g of the continuous background in the spatial Fourier spectra of the Th–Mo structures as a function of b. s is minimal near the optimal value of b where Q_h is maximal. g decreases monotonously as b increases.

Several types of high-Q modes are identified in the frequency range $0.2<a/\lambda<0.5$, each has a distinct field distribution. Figure 3(c) shows the spatial distribution of magnetic field for three types of modes, labeled as I, II, and III. As b increases, different modes become the highest-Q modes within the frequency range of interest. For example, when b is close to 0, type I [squares in Fig. 3(a)] is the highest-Q mode. For $0.37<b<0.75$, type II (triangles) takes over. At $b=0.88$, type III mode (circles) has the maximal Q. We trace the change in Q factor for each type of modes as b varies. Figure 3(b) plots the Q values for type II and III modes as a function of b. With increasing b, the Q of type II first increases, reaches the maximum at $b=0.75$ and then decreases. Type III exhibits a similar trend but reaches the maximal Q at a larger value of b. Hence, the Q factors for different modes are maximized at different b. Typically the higher Q modes have lower lasing threshold, thus we may choose different types of modes for lasing by varying b.

To understand why Q is maximal at an intermediate value of b, we analyze light leakage from the structure. In a free-standing membrane, light can leak either horizontally from the edge of the pattern or vertically to the air above or below. These two leakage rates are characterized by Q_h^{-1} and Q_v^{-1}, respectively. The total leakage rate is $Q^{-1}=Q_h^{-1}+Q_v^{-1}$. In Fig. 4(a), we plot Q_h and Q_v for the highest-Q modes as a function of b. While Q_v increases monotonically with b, Q_h is peaked near the optimal value of b. The variation in Q_h is associated with the change in mode size $s\equiv L^2\int I(x,y)^2dxdy/[\int I(x,y)dxdy]^2$, where $I(x,y)$ is the spatial distribution of field intensity and L is the lateral dimension of the structure. As shown in Fig. 4(b), s reaches the minimum at $b=0.75$. This can be seen from the field patterns in Fig. 3. The type II mode is more confined horizontally than types I and III, thus it has smaller light leakage through the pattern boundary and higher Q_h. The trend of s with b can be understood qualitatively from the PBG effect. In the periodic structure $b=1$, the high-Q modes are band edge modes which are spatially extended and have large s. When the structural aperiodicity is introduced $b<1$, defect modes are formed in the PBG and become localized. As b decreases, the defect modes move from the edge to the center of the gap. The mode size s decreases because light confinement is the strongest at the gap center. However, the structural aperiodicity reduces the PBG. When b is small enough, the gap closes and s increases. Hence, there is an optimal value of b where s is the minimal. The variation in Q_v with b can be explained by the change in spatial Fourier power spectra of the structure. The spatial Fourier spectrum of the Th–Mo structure is singular continuous. The continuous background provides spatial frequencies that allow light of any horizontal k vector outside the light cone being scattered into the light cone and then leaking vertically out of the membrane. As b increases, the continuous background reduces (Fig. 1). Consequently the vertical leakage decreases and Q_v increases. This is confirmed by the percentage g of the continuous background computed from the spatial Fourier spectra. As plotted in Fig. 4(b), g drops continuously with increasing b.

In summary, we have demonstrated lasing action in quasi-2D Thue–Morse structures that are fabricated in a GaAs membrane. By changing the relative size of two scatterers that correspond to the building blocks A and B, we gradually vary the degree of aperiodicity and investigate its effect on lasing. There exists an optimal degree of aperiodicity where the quality factor reaches a global maximum and lasing becomes the strongest. This is attributed to an enhancement of horizontal confinement of light in a finite-size pattern by structural aperiodicity. However, the continuous background in the spatial Fourier spectrum of the Thue–Morse structure facilitates vertical leakage of light out of the membrane. At various degrees of aperiodicity, different types of modes acquire the highest quality factors and may be selected for lasing. This opens a way of controlling lasing characteristic via structural aperiodicity.

This work was partially supported by the NSF (Grant No. DMR-0808937), the U.S. Air Force Award (Grant No. FA9550-10-1-0019), and the NSF Career Award (Grant No. ECCS-0846651).

[1]E. Maciá, Rep. Prog. Phys. **69**, 397 (2006).
[2]N. Poddubny and E. L. Ivchenko, Physica E **42**, 1871 (2010).
[3]M. Kolář, M. K. Ali, and F. Nori, Phys. Rev. B **43**, 1034 (1991).
[4]N. H. Liu, Phys. Rev. B **55**, 3543 (1997).
[5]X. Jiang, Y. Zhang, S. Feng, K. C. Huang, Y. Yi, and J. D. Joannopoulos, Appl. Phys. Lett. **86**, 201110 (2005).
[6]G. Gumbs, G. S. Dubey, A. Salman, B. S. Mahmoud, and D. Huang, Phys. Rev. B **52**, 210 (1995).
[7]F. Iglói, L. Turban, and H. Rieger, Phys. Rev. E **59**, 1465 (1999).
[8]F. Qiu, R. W. Peng, X. Q. Huang, Y. M. Liu, M. Wang, A. Hu, and S. S. Jiang, Europhys. Lett. **63**, 853 (2003).
[9]L. Dal Negro, M. Stolfi, Y. Yi, J. Michel, X. Duan, L. C. Kimerling, J. LeBlanc, and J. Haavisto, Appl. Phys. Lett. **84**, 5186 (2004).
[10]L. Dal Negro, J. H. Yi, V. Nguyen, Y. Yi, J. Michel, and L. C. Kimerling, Appl. Phys. Lett. **86**, 261905 (2005).
[11]F. Qiu, R. W. Peng, X. Q. Huang, X. F. Hu, M. Wang, A. Hu, S. S. Jiang, and D. Feng, Europhys. Lett. **68**, 658 (2004).
[12]A. Barbé and F. Von Haeseler, Int. J. Bifur. Chaos **17**, 1265 (2007).
[13]L. Dal Negro, N. N. Feng, and A. Gopinath, J. Opt. A: Pure Appl. Opt. **10**, 064013 (2008).
[14]L. Moretti and V. Mocella, Opt. Express **15**, 15314 (2007).
[15]S. V. Boriskina, A. Gopinath, and L. Dal Negro, Opt. Express **16**, 18813 (2008).
[16]J. K. Yang, S. V. Boriskina, H. Noh, M. J. Rooks, G. S. Solomon, L. Dal Negro, and H. Cao, Appl. Phys. Lett. **97**, 223101 (2010).